CHEMICAL AND PROCESS ENGINEERING
2010, 31, 579–588

HENRYK KUDELA*, TOMASZ KOZŁOWSKI

HYDRODYNAMIC EFFECTS PRODUCED BY PLUNGING FOIL IN A FLUID

Wroclaw University of Technology, Department of Numerical Fluid Flow Modelling,
Wybrzeże Wyspiańskiego 50-370 Wrocław, Poland

Numerical results have been presented related to unsteady effects produced by oscillating foil in fluids. The paper was inspired by the studies over insects and birds fly. It was shown that by choosing the frequency and amplitude of oscillations various kinds of the vortex Karman street can be generated and this way controlling of the drag, lift and thrust force exerted on the object may be possible. For numerical study, the vortex in cell method has been used. Dependences of the amplitude of oscillations and vortices topology on the Strouhal number have been established behind the oscillating foil by constructing the phase space diagram. The computational results are consistent with the available experimental data.

Przedstawiono wyniki badań numerycznych efektów hydrodynamicznych wywołanych ruchem drgającym prostym profilu w płynie. Praca była inspirowana badaniami eksperymentalnymi i numerycznymi aerodynamiki lotu ptaków i owadów. Pokazano, że przez odpowiedni dobór parametrów ruchu profilu, takich jak częstotliwość oscylacji i ich amplituda można wywoływać i modyfikować ślad aerodynamiczny za profilem. Odnosi się to do położenia wirów ścieżki wirowej. Zmiana ich położenia powoduje zmianę siły oporu, siły nośnej i siły przyspieszającej. Do badań numerycznych wykorzystano metodę cząstek wirowych. Skonstruowano diagram fazowy na płaszczyźnie parametrów, z którego łatwo można wyznaczyć typ ścieżki wirowej dla zadanej wartości amplitudy drgań i częstotliwości. Wyniki badań numerycznych pozostają w dobrej zgodności z danymi eksperymentalnymi dostępnymi w literaturze.

1. INTRODUCTION

A great interest in the low Reynolds number unsteady aerodynamics of oscillating foil stems from increasing importance of micro air vehicles and from the will to understand the aerodynamics of natural flyers. Flapping motion is a basic mode of locomotion in birds, insects and fishes. The basic question is how they generate enough lift and the thrust force to be able to perform remarkable manoeuvres with rapid accelerations and decelerations. From the point of the fluid mechanics we believe that all the

*Corresponding author, e-mail: henryk.kudela@pwr.wroc.pl

phenomena related to the generation of hydrodynamic forces are ruled by the dynamics of the vorticity. The Karman vortex street in a flow over a steady profile generates a drag force. On the other side, the flapping motion of the profile may reverse Karman vortex street producing the thrust force. In the paper, production of the lift and thrust forces has been demonstrated for the basic two dimensional oscillating foil. Although flight in nature is naturally three-dimensional, when the ratio of the span to the chord is large enough, the two-dimensional model may be used [11–15]. It is believed that 2D model allows one to capture the essence of flapping flight hydrodynamics. The primary parameter characterizing the oscillating foil is amplitude of the oscillation (A_C), the Strouhal (St_A) and Reynolds numbers (Re). We demonstrated dependences between these basic parameters and vortex wake topology, the reversing of the topology of the vortex Karman street and deflection of its from the main direction of the flow. These phenomena directly influenced production of the thrust and lift forces. For numerical study, we chose the vortex in cell (VIC) method. The importance of the method lies in the possibility of the analyzing more easily and directly the vorticity field due to the fact that in computation vortex particles carrying the information about the vorticity field are used. Attractive feature of the method is also the elimination of pressure from the equation of the fluid motion.

2. VORTEX IN CELL METHOD

2.1. GOVERNING EQUATIONS

The Navier–Stokes equation in primitive variables with the coordinates fixed to the moving body has the form [14]

$$\frac{\partial u}{\partial t}+\nabla u\cdot u=-\nabla p+\nu\Delta u-\frac{\partial U_0}{\partial t}+\left[-\frac{\partial \Omega_0}{\partial t}\times r+2\Omega_0\times u+\Omega_0\times(\Omega_0\times r)\right] \quad (1)$$

$$\nabla\cdot u=0 \quad (2)$$

where Ω_0 and U_0 are the angular translation velocity vectors of the wing. The last three terms in Eq. (1) arise from non-inertial coordinate system and denote non-inertial force due to rotational acceleration, the Coriolis force and the centrifugal force, respectively. Taking the curl by the both sides of the Eq. (1) and assuming 2D flow, the evolution equation for the vorticity in the reference system fixed to moving body, one can transform to the form [6]

$$\frac{\partial(\omega^*)}{\partial t}+\nabla\omega^* u=\nu\Delta\omega^* \quad (3)$$

$$\Delta\psi^*=-\omega^* \quad (4)$$

$$u = \nabla \times (0, 0, \psi^*) \tag{5}$$

where $\omega^* = \omega + 2\Omega_0$, $\psi^* = \psi - \psi_\infty$ and stream function far from the body, at the infinity ψ_∞ take the form $\psi_\infty = U_0(y\cos\alpha - x\sin\alpha) - (\Omega_0/2)(x^2+y^2)$. Further, the star index (*) was dropped. A detailed description of solution of the Helmholtz equations in moving reference frame can be found in [6].

2.2. VORTEX IN CELL METHOD FOR CONFORMAL GEOMETRY

In order to better fit a numerical grid to a solid boundary, we transform the non-rectangular physical region (x, y) variables to the rectangular one (ζ, η). The following conformal transformation was applied (Fig. 1)

$$x + iy = \cosh(\zeta + i\eta) \tag{6}$$

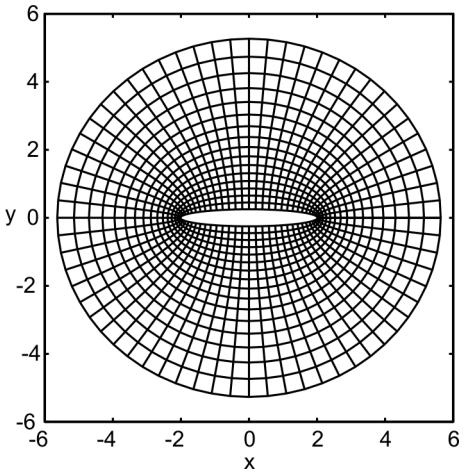

Fig. 1. Elliptical grid in the physical domain

In new variables (ζ, η), Eqs. (3), (4) take the form

$$\frac{\partial \omega}{\partial t} + \nabla\omega \cdot u = \frac{\nu}{J}\Delta\omega \tag{7}$$

$$\Delta\psi = -\omega, \qquad u = \frac{1}{J}\frac{\partial \psi}{\partial \eta}, \qquad v = -\frac{1}{J}\frac{\partial \psi}{\partial \zeta} \tag{8}$$

where J denotes the Jacobian of the conformal transformation. The nullifying of the normal velocity component is obtained by setting ψ = const on the wall. The no-slip condition is realized by introducing a proper portion of vorticity, that ensures the condition $u \cdot \mathbf{s^0} = 0$, were $\mathbf{s^0}$ is a tangential unit vector [8, 16]. In the VIC method, the con-

tinuous vorticity field is approximated with a discrete vortex particles distribution. The flow region is covered with the numerical grid (*ih, jh), h* = $\Delta\eta = \Delta\zeta$. In every grid node (*i,j*), the particles with circulation $\Gamma_{ij} = \int_A \omega d\zeta d\eta$ are placed, where $A = h^2$ and

$$\omega(\zeta,\eta) = \sum_{i,j} \Gamma_{ij}\delta(\zeta - \zeta_i)\delta(\eta - \eta_j) \tag{9}$$

The viscous splitting algorithm [3] was used for solution of Eqs. (7), (8). At first, the inviscid fluid motion equation was solved

$$\frac{\partial\omega}{\partial t} + \nabla\omega \cdot u = 0 \tag{10}$$

It stems from Eq. (11) that vorticity is constant along the trajectory of the fluid particles. According to the Helmholtz theorem [18], vortex particles are moving like material fluid particles. The differential equation (Eq. (10)) is replaced by the set of ordinary equations

$$\frac{d\zeta}{dt} = u, \quad \frac{d\eta}{dt} = v, \quad \zeta(0) = \alpha_1, \quad \eta(0) = \alpha_2 \tag{11}$$

where $\alpha = (\alpha_1, \alpha_2) = (\zeta_i, \eta_j)$ means the Lagrangian coordinate of fluid particles. The number of particles is equal to the number of grid nodes. The finite set of Eqs. (11) was solved by the fourth order Runge–Kutta method. The velocity field was obtained by solving the Poisson equation (8) on the numerical grid. The velocities of the particles between the grid nodes were calculated by the two dimensional bilinear interpolation.

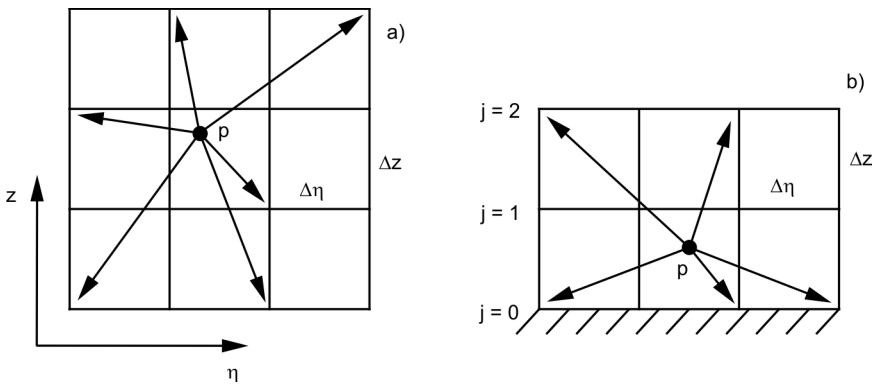

Fig. 2. Redistribution of the particle masses onto neighbouring grid nodes:
a) for particles lying inside the computational domain (at least one cell from the wall),
b) for particles in the vicinity of a wall

At the second step, the viscosity was taken into account. The diffusion equation was solved

$$\frac{\partial \omega}{\partial t} = \frac{\nu}{J} \Delta \omega, \qquad \omega(\zeta, \eta) = 0 \;\; \omega|_{\text{wall}} = \omega_s \tag{12}$$

where ω_s was calculated based on the Poisson equation (8). The non-slip condition $u = 0$ is realized by adding proper value of the vorticity on the wall ω_s [16].

After displacement of particles according to Eq. (11), one has to redistribute the mass of the particles to the grid nodes (Fig. 2). It was done, according to the formula

$$\omega_{ij} = \frac{1}{h^2} \sum_p \Gamma_p \phi_h(\zeta)\, \phi_h(\eta) \tag{13}$$

where $\varphi_h(\cdot)$ denotes the kernel of the interpolation function. Interpolation of particle masses onto the grid nodes has a fundamental meaning for the precision of the VIC method. In the present work, the redistribution process was performed using Z-splines [2]. After redistribution, the diffusion equation (12) was solved on the numerical grid, with alternating direction implicit (ADI) scheme [13]. Detailed numerical test of the VIC method can be found in [9, 10].

3. NUMERICAL SIMULATION

3.1. FORMULATION OF THE PROBLEM AND COMPUTATION DETAILS

The elliptic foil was used with prescribed motion in the vertical direction according to the equation

$$y(t) = \frac{A_0}{2} \cos(2\pi f t) \quad u = \frac{dy}{dt} \tag{14}$$

where $y(t)$ denotes instantaneous position of the wing centre, A_0 is the amplitude, f is the frequency of the oscillation and u denotes the airfoil vertical velocity. Far from the body, the velocity of the fluid U_0 was assumed to be constant (Fig. 3). The motion of the profile described by Eq. (14) is known as a plunging one. The phenomena related to the plunging foil can be characterized by three non-dimensional numbers: *Re* – Reynolds number, *St* – Strouhal number and non-dimensional amplitude of plunging A_C, [1, 4, 5]:

$$Re = \frac{U_0 c}{\nu}, \quad St = \frac{fc}{U_0}, \qquad A_C = \frac{A_0}{c} \tag{15}$$

where c is the chord of the foil and ν is the kinematic coefficient of fluid viscosity

The chord was set to $c = 2$ and thickness of the profile $e = 0.4$. We perform the calculations for the constant Reynolds number $Re = 100$ and homogeneous fluid with the density $\rho = 1$. The plunging frequency was fixed to $f = 0.5$ and the Strouhal num-

ber St was changed by varying the free stream velocity U_0. The calculations were carried on for dimensionless time $T = ft$, in range $T = (0, 10)$.

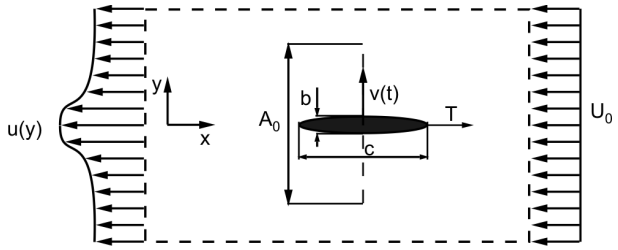

Fig. 3. Scheme of the plunging airfoil immersed in the fluid

In calculations, an elliptical mesh, shown in Fig. 1 was used, with 256 grid nodes in the radial direction and 256 grid nodes in the azimuth direction. A constant time step Δt was set to 0.01.

3.1. NUMERICAL RESULTS

It is well known that hydrodynamic forces exerted on the moving body immersed in a fluid can be described by the dynamics of vorticity [17, 18]. By a proper choice of the frequency and amplitude of plunging we can change the position of the vortices in the vortex street.

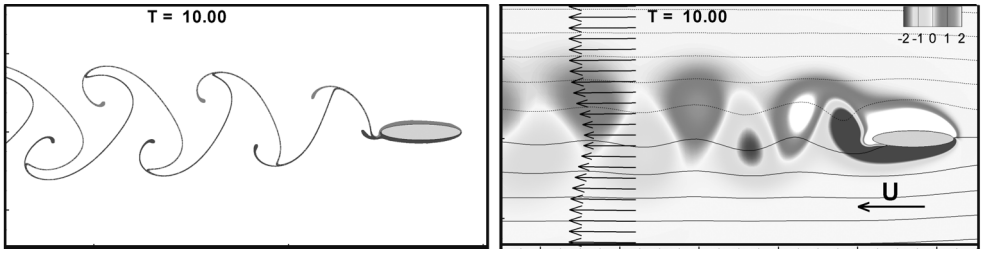

Fig. 4. Vortex Karman street produced by plunging foil with $St = 0.6$ and $A_C = 0.25$. The arrows behind the airfoil denote averaged fluid velocity profiles. The arrow on the bottom right corresponds to the value of the free stream velocity U_0. In Fig. 9 this case is represented by squares

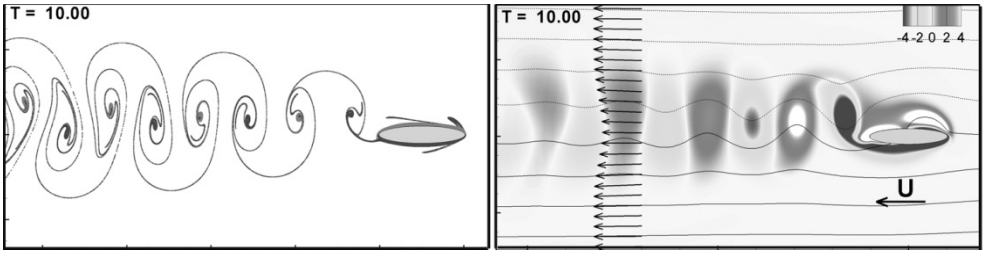

Fig. 5. Aligned vortices, $St = 0.8$ and $A_C = 0.5$, in Fig. 9, denoted by full squares

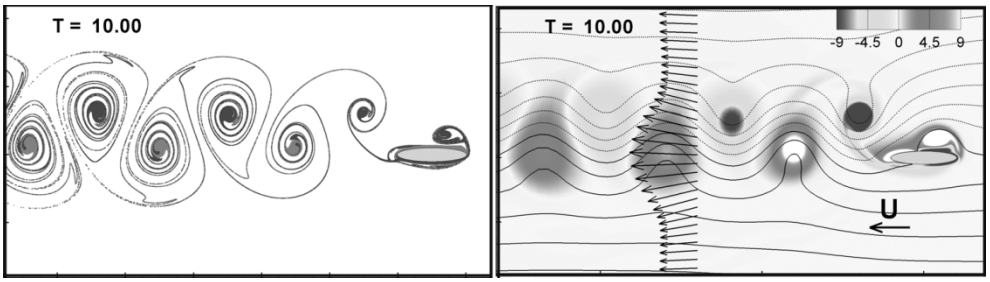

Fig. 6. The reversed Karman vortex street, St = 0.8 and A_C = 0.75 (rvKs),in Fig.9 denoted by crosses

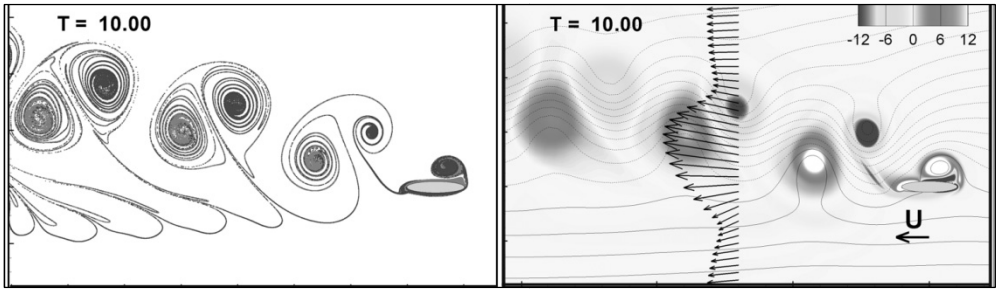

Fig. 7. Deflected reverse vortex Karman (drvKs) St = 0.8 and A_C = 1.0, in Fig. 9 denoted by triangles

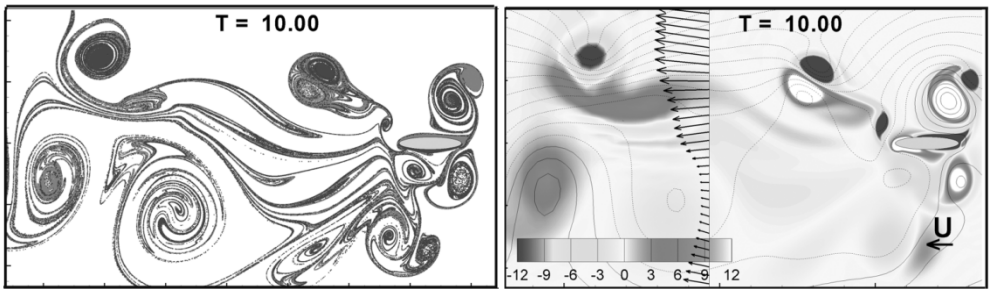

Fig. 8. Random vorticity field , St = 1.2 and A_C = 1.0, in Fig. 9 marked by full circles

In Figures 4–8, various kinds of the vortex streets were shown. In Figure 4 (St = 0.6, A_C = 0.25), the vortex Karman street (vKs) is presented. On the left side of Fig. 4, the vortex street was visualized by streak lines (passive particle that was taken by fluid from the surface of the profiles). On the right part of the figure, the flow is visualized by vorticity distribution and streamlines. Mean velocity profiles behind the foils are also shown. By the vortex Karman street, we mean the vortex street when the vortices shed form the upper (lower) side of the profile stay on the upper (lower) side of the axis of symmetry. The situation presented in Fig. 5 (St = 0.8, A_C = 0.5) is called align vortices (av). It means that the vortices are placed on the axis of symmetry. The drag force ($F_D = C_D \rho U_0^2 A/2$), where C_D means the drag force coefficient, was dropped but is not equal zero. It is a transitional state of the vortex street.

Increase of the plunging amplitude (St = 0.8, A_C = 0.75) leads to the reverse vortex street (Fig. 6). The vortices shaded on the upper surface of the profile changed the position and went to the below of symmetry axis. The vortices created on the lower part of the profile surface went to the upper positions. In such a configuration, the thrust force was produced ($C_D < 0$). For inverse vortex street state, one can find the parameters for that the drag force was equal zero. Further increase the plunging amplitude (St = 0.8, A_C = 1.0) leads to the deflection of the reverse Karman vortex street (drvKs) resulting in production of the lift force (Fig. 7). In Figure 8, it is shown that for (St = 1.2, A_C = 1.0), a random vortex street was obtained. It is worth noting that in this regime the manoeuvrability will be difficult due to the random distribution of hydrodynamic forces on the profile.

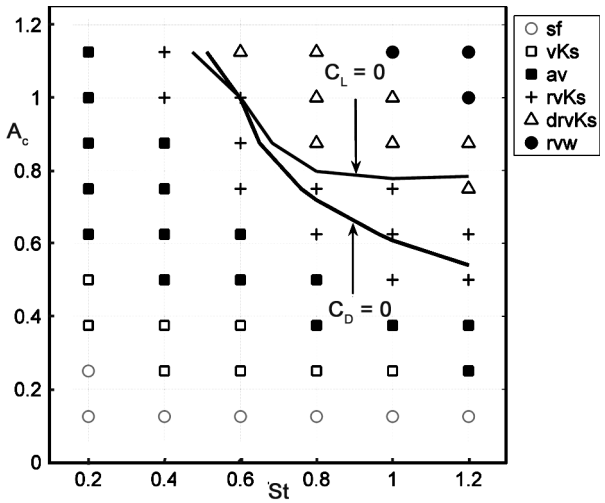

Fig. 9. Dependences of non-dimensional plunging amplitude A_C
and vortex topology in the wake behind of the foil on the Strouhal number St, Re = 100;
symbols denote: ○ – steady vortex bubbles, □ – vortex Karman street (vKs),
■ – transition region with aligned vortices (av), + – reversed vortex Karman street (rvKs),
Δ – deflected reverse Karman vortex street, ● – random vortex wake

The above results may be summarized in phase space diagrams. In Figure 9, the dependence of the wake type on Strouhal number St and amplitude of oscillation is presented. For a given Reynolds number Re = 100, at a small amplitude of oscillations, we observed the stationary vortex bubbles behind the foil. They are attached to the profiles. This regime marked by circles (○) in Fig. 9 is independent of the Strouhal number. If the amplitude of oscillation increases, the vortex bubbles are no longer stationary, forming a Karman vortex street behind the body, denoted by empty squares (□). The vortices reduce fluid momentum in the profile wake causing the drag production ($C_D > 0$). The transitional region marked by full squares (■) is related to the situation when opposite vortices form a row behind the profile of aligned vortices

(av). Inversion of the topology of the vortices (Fig. 6) led to the revere vortex Karman street (rvKs) that results in the production of a thrust force. The counter-rotating vortices in the foil wake increase the fluid momentum forming jet flow. However generation of the thrust force is not obligatory for this type of the wing wake topology. In Figure 9, the curve for $C_D = 0$ is depicted. Only over the curve, the thrust force is generated ($C_D < 0$).

If the Strouhal number and amplitude of oscillations increase, the symmetry of the wake is broken and the deflection of the vortex Karman street (drvKs) from horizontal direction is observed. This phenomenon is related to the lift force production [7]. As for the thrust force, the positive lift force appears over the curve with $C_L = 0$. Further increase of the Strouhal number and amplitude of oscillations results in a random vorticity field generation A similar phase space diagram for (St, A_C) was obtained experimentally for a pitching profile [4, 5].

3. CONCLUSIONS

The Vortex-In-Cell method was used to model the hydrodynamics effect of the plunging foil. Despite of the 2D fluid flow simplification, the dynamics of fluid motion is very reach and permit to understand the non-linear nature of the flapping effect and the structure of the vorticity flow. The dynamics of the vorticity field is responsible for production of the lift and thrust forces during the flight of the natural flyers. The computational result are in qualitative agreement with experimental data presented in [4], [5], although we assumed much smaller Reynolds number and perform the basic plunging motion of the profile.

SYMBOLS

ω – z-direction component of the vorticity field
ψ – stream function
$\mathbf{u}$ – fluid velocity vector
A_0 – amplitude of profile oscillations
f – frequency of oscillations
c – chord length
U_0 – free stream velocity
St_A – Strouchal number defined with respect to the amplitude of oscillation
St – Strouchal number with respect to the chord length
$C_{D,L}$ – drag and lift coefficient respectively

REFERENCES

[1] ANDERSON J. M., STREITLIEN K., BARRET D.S., TRIANTAFYLLOU M.S., J. Fluid. Mech., 360, 1998, 41.
[2] BECERRA SAGREDO, *Moment conserving Cardinal Splines Interpolation of Compact Support for Arbitrarily Spaced Data*, Research Report No. 10, Zurich, Switzerland, 2003.
[3] COTTET G-H., KOUMOUTSAKOS P., V*ortex Methods Theory and Practice*, Cambridge University Press, Cambridge, 2000.
[4] GODOY-DIANA R., AIDER J-L.,WESFREID J., E., Physical Rev. E, 2008, 77, 016308.

[5] GODOY-DIANA R., MARAIS C., AIDER J-L., WESFREID J., E., J. Fluid Mech., 2009, 622, 23.
[6] GUSTAFSON K.E., LEBEN R., FREYMUTH P., *Vortex methods and vortex motion*, Philadelphia, PA, Society for Industrial and Applied Mathematics, 1991, 143.
[7] JONES K.D., DOHRING C.M., PLATZER M.F., AIAA, 1996, 96-0078.
[8] KOUMOUTSAKOS P., LEONARD A., PEPIN F., J. Comp. Phys., 1994, 113, 52.
[9] KUDELA H., MALECHA Z.M., Task Quarterly, 2009, 13, 15.
[10] KUDELA H., KOZLOWSKI T., J. Theor. Appl. Mech., 2009, 47, 779.
[11] PESKIN CH.,S., MILLER L.A., J. Exp. Biol., 2004, 207, 3073.
[12] SHYY W., LIAN Y., TANG J., VIIERU D., LIU H., *Aerodynamics of Low Reynolds Number Flyers* Dover Publications, Dover Publications, Cambridge University Press, 2008.
[13] THOMAS J.W., *Numerical Partial Differential Equations: Finite Difference Methods*, Springer, 1995.
[14] WANG Z., J., J. Exp. Biol., 2004, 207, 4147.
[15] WANG Z.J., BIRCH J.M., DICKINSON M.HJ. Exp. Biol., 2000, 207, 449.
[16] WEINAN E., JIAN-GUO LIU., J. Comp. Phys., 1996,124, 368.
[17] WU J.C., AIAA, 1981, 19, 432.
[18] WU J Z., MA H.Y., ZHOU M.D., *Vorticity and Vortex Dynamics*, Springer, 2005.

EFEKTY HYDRODYNAMICZNE GENEROWANE PRZEZ OSCYLUJĄCY PROFIL

Przedstawiono wyniki badań numerycznych efektów hydrodynamicznych wywołanych ruchem drgającym prostym w płynie. Praca była inspirowana badaniami eksperymentalnymi oraz badaniami numerycznymi aerodynamiki lotu ptaków i owadów. Do badań numerycznych założono, że przepływ wokół oscylującego ciała jest dwuwymiarowy. Jest to założenie ogólnie stosowane, gdy stosunek rozpiętości skrzydła do jego cięciwy jest odpowiednio duży. Przyjęto, że oscylacyjny ruch profilu i jego prędkość są zadane, a ruch odbywa się w kierunku prostopadłym do kierunku napływu. Pokazano, że przez odpowiedni dobór parametrów ruchu, takich jak częstotliwość oscylacji i amplituda, można wywoływać i modyfikować ślad aerodynamiczny za profilem. Odnosi się to do położenia struktur wirowych w śladzie aerodynamicznym. Wyróżniono następujące typy ścieżki wirowej: klasyczna ścieżka wirowa Karmana, ścieżka Karmana z ułożonymi w linii prostej strukturami wirowymi, odwrócona ścieżka Karmana, odchylona ścieżka Karmana oraz chaotyczny ślad wirowy. Zmiana położenia wirów w ścieżce wirowej powoduje zmianę siły oporu, siły nośnej lub siły przyspieszającej. Do badań numerycznych wykorzystano metodę cząstek wirowych typu cząstka wirowa w komórce. Metoda opiera się na algorytmie dekompozycji lepkościowej. Rozwiązanie otrzymuje się w dwóch krokach: najpierw rozwiązuje się równanie bez uwzględnienia lepkości, a następnie uwzględnia się lepkość płynu przez rozwiązanie równania dyfuzji. Warunek przylegania płynu do ściany sztywnej realizuje się przez generację odpowiedniej porcji wirowości. Aby dopasować siatkę numeryczną do kształtów profilu, posłużono się odwzorowaniem konforemnym. Ze względu na wirowy charakter zjawisk wokół profilu metoda cząstek wirowych okazała się wyjątkowo skuteczna i dokładna. Skonstruowano diagram fazowy oparty na liczbie Strouhala (St) i amplitudzie (A_C) oscylacji. Z diagramu można łatwo wyznaczyć charakter ścieżki wirowej dla zadanej wartości amplitudy drgań i częstotliwości. Przedstawione wyniki obliczeń są w dobrej zgodności z danymi eksperymentalnymi dostępnymi w literaturze.

Received 24 August 2010